Thrust Force Vibration Suppression of Drone Rotor by Higher Harmonic Rotational Speed Control

Yuto Naoki[1], Sakahisa Nagai[2] and Hiroshi Fujimoto[2]

Abstract— **Recent advancements in unmanned aerial vehicle (UAV) and multirotor technology have increased industrial applications, but safety and noise remain challenges. The aim is to devise a method to suppress thrust force vibration in crosswind conditions that apply to small-sized multirotors. A higher harmonic rotational speed control method is proposed based on the position-dependent aerodynamic force model. Second-order harmonic thrust vibration under crosswind conditions is simply modeled, and higher harmonic input is designed only for use in the rotational speed and utilized high torque response performance of the electric motor. The effectiveness of the proposed method is validated through the wind tunnel experiment.**

I. INTRODUCTION

The development and industrial applications of UAVs, such as drones and manned multirotor aircraft, have advanced in recent years [1] . However, safety and noise are the problems hindering their widespread adoption [2] and the research aimed at improving safety has been conducted from the motor level to the aircraft level [3]. Remarkably, the significant vibration and noise levels directly affect safety and precision performance in industrial applications such as observations and transports.

Vibration suppression in existing aircraft with propeller rotors can be classified into the passive method by design, the addition of dampers [4], and the active method by control using actuators. The same classification applies to multirotor aircraft. Research working on active methods in drones includes position control by virtually simulating a dynamic vibration absorber [5], nonlinear control based on the backstepping method focusing on the vibration caused by the elastic properties of the frame of the quadrotors [6], and the study on optimizing the distribution of multiple rotors for torsional elastic vibration of an articulated aerial robot [7]. These methods aim to avoid transmitting vibrations from the vibration source to the airframe.

Various vibrational sources have been assumed, such as human or autonomous control navigation, environmental disturbances, and propulsion systems, such as engines and motors. In aircraft, the aerodynamic effects on the disturbance or propulsion systems are unique problems, and the research has been conducted on aircraft level [8]. Suppressing the propulsion systems' vibration could be a fundamental solution to vibration.

*This work was partly supported by JSPS KAKENHI Grant Number JP23H00175.

[1]Y. Naoki is with Graduate School of Engineering, The University of Tokyo, Chiba, 277-8561, Japan

[2]S. Nagai and H. Fujimoto are with Graduate School of Frontier Science, The University of Tokyo, Chiba, 277-8561, Japan

In a multirotor aircraft utilizing rotating propeller rotors as propulsion systems, the vibrations are inherent due to the rotational nature of the propellers. In the conventional aircraft like airplanes and helicopters, the propeller vibrations are generally categorized into mechanical, dynamic, and aerodynamic imbalances. Mainly, aerodynamic imbalance presents unique challenges associated with propellers. For instance, effects such as lift and torque imbalance within the plane of rotation due to crosswind can cause vibrations proportional to the rotational speed. Additionally, helicopters exhibit higher-order rotational noise proportional to the rotational speed, including blade inherent vibrations, aerodynamic excitation, and higher-frequency rotational noise such as Blade/Vortex Interaction (BVI) noise generated when blade wakes interact with trailing vortices during descent. It is assumed that the vibrations caused by aerodynamic force will also be significant in UAVs, which are the focus of this study.

Regarding rotor vibration suppression control in aircraft other than multirotor aircraft, the most prominent examples are higher harmonic control (HHC) and individual blade control (IBC) in helicopters [9]. These techniques aim to mitigate rotor vibrations dependent on rotational speed by superimposing high-frequency inputs on cyclic pitch (variable pitch) control of the helicopter rotor to distribute the position-dependent pressure in the plane of rotation. Typical HHC methods use H_2 control [10], and research on system identification by black box modeling using a learning-based method with a large amount of flight data is recently conducted [10]. In recent years, with the complete electrification of helicopters, there have been cases where attempts to apply IBCs while adopting simpler structures [11].

However, the traditional HHCs and IBCs require the addition of hydraulic actuators to the mechanisms, and due to their complexity, there are few examples of practical application. On the other hand, in drones and multirotor aircraft, passive mechanisms are used to cope with vibrations due to attitude control based on rotational speed and by their size and high rotational speed. However, as the demand for further performance improvement grows with the increase in size and industrial applications, rotor vibration suppression becomes inevitable.

Therefore, this study aims to devise a method to suppress vibration using only the rotational speed control of a rotor. The vibration suppression method using harmonic input is a primary technique for mitigating torque ripples [12] and mechanical vibrations [13]. This paper focuses on the thrust vibration of a single rotor under crosswind inflow as a condition that causes significant vibration while the

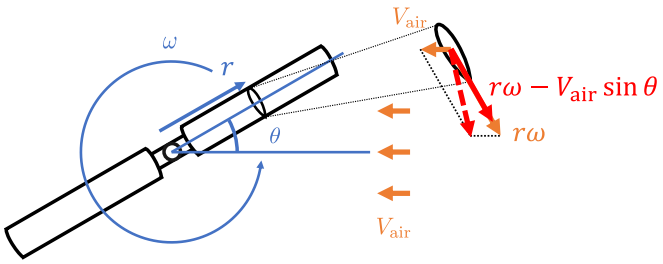

Fig. 1. The wind vector acting on the wing element. The left side is a top view, and the right side is a zoomed-in view.

motor vibration itself are assumed to be small enough. The precise thrust control using only rotational speed under conditions of various flows, including crosswind, has been studied [14]. However, high-frequency vibrations have not been considered. The rotor thrust vibration of a multirotor, which has not been suppressed, is aerodynamically modeled considering crosswind inflow based on the blade element theory, and a suppression method is proposed using harmonic rotational speed inputs. The contributions of this research are the derivation of a vibration model of the thrust during crosswind inflow and the proposal of a harmonic vibration suppression method at rotational speed by utilizing the high-torque response characteristics of the electric motor.

The outline of this paper is as follows: In Section II, crosswind vibration is first modelled theoretically as an aerodynamic vibration, and then a vibration suppression method with harmonic speed inputs based on the model is proposed. In Section III, the effectiveness of the proposed method is verified by wind tunnel tests and the results are presented and discussed. In Section IV, the performance improvement with the developed approach is experimentally validated. In Section V, conclusions are presented.

II. Methods

A. Modeling of thrust force vibration in cross wind condition

To formulate the problem, we theoretically model the vibration induced by crosswind flow. Here, the crosswind is the wind which is parallel to the plane of rotation, assumed to be generated by environmental disturbances or air speed of the aircraft. The forces acting on the blade are explained by the blade element theory, considering the force over a small interval from the center of the blade r to $r + \mathrm{d}r$. Here, we assume that only the perpendicular component of the airspeed V_{air} relative to the blade affects the force, and the other elements, including polar direction and vertical inflow, are ignored. A model of the wind vector affecting the propeller blade during crosswind flow is shown in Fig. 1. The position of the blades is expressed by a phase θ with the flow direction as $0\,\mathrm{deg}$. The number of blades is considered as $b = 2$, which is used in common small propellers. The perpendicular flow velocity at the blade element part $V_\perp$ is

$$V_\perp = r\omega - V_{\text{air}} \sin\theta. \tag{1}$$

Therefore, the force $\mathrm{d}F$ in the direction of rotor thrust on the blade element coincides with the lift $\mathrm{d}L$ of the blade element and written as

$$\mathrm{d}F = \mathrm{d}L = \frac{1}{2}\rho(r\omega - V_{\text{air}} \sin\theta)^2 C_L C \mathrm{d}r \tag{2}$$

where ρ is the air density, ω is the rotational speed, C_L is the lift coefficient and C is the chord length. The thrust on the blade can be calculated by integrating $\mathrm{d}F$ up to the blade length R for position r. In the case of a two-blade propeller, the phases differ by 180° thus the thrust on each blade can be calculated as

$$F_1 = \frac{1}{2}\rho C_L C \left(\frac{1}{3}\omega^2 R^3 - \omega R^2 V_{\text{air}} \sin\theta + R V_{\text{air}}^2 \sin^2\theta\right) \tag{3}$$

$$F_2 = \frac{1}{2}\rho C_L C \left(\frac{1}{3}\omega^2 R^3 + \omega R^2 V_{\text{air}} \sin\theta + R V_{\text{air}}^2 \sin^2\theta\right) \tag{4}$$

Therefore, the vibration of the thrust in the direction of the rotation axis $F_z = F_1 + F_2$ is expressed as

$$F_z = \rho C_L C \left(\frac{1}{3}\omega^2 R^3 + R V_{\text{air}}^2 \sin^2\theta\right) \tag{5}$$

$$= \rho C_L C \left(\frac{1}{3}\omega^2 R^3 + \frac{1}{2} R V_{\text{air}}^2 (1 - \cos 2\theta)\right). \tag{6}$$

It can be seen that both the steady-state and the vibratory components are added due to the crosswind.

B. Vibration suppression by higher harmonic rotational speed control

This paper proposes the thrust vibration suppression by the rotational speed control. If we input a fixed rotational speed ω_0 and a periodic waveform synchronized with it in frequency into the thrust F_z model (6) considering the effect of crosswind inflow, then the input can be expressed as

$$\omega = \omega_0 + A\cos 2\omega_0 t \tag{7}$$

$$\theta = \omega t \approx \omega_0 t \tag{8}$$

where A is the amplitude of the periodic waveform. By substituting (7) into (6), the thrust can be calculated as

$$F_z = \rho C_L C \left(\frac{1}{3}(\omega_0 + A\cos 2\omega_0 t)^2 R^3 \right. \tag{9}$$

$$\left. + \frac{1}{2} V_{\text{air}} R (1 - \cos 2\omega_0 t)\right) \tag{10}$$

$$= F_{z0} + F_{z\theta} \tag{11}$$

where the steady-state component F_{z0} and the vibratory component $F_{z\theta}$ are

$$F_{z0} = \frac{1}{6}\rho C_L C \left(2R^3\omega_0^2 + 3RV_{\text{air}}^2\right) \tag{12}$$

$$F_{z\theta} = \frac{1}{6}\rho C_L C \left((4R^3\omega_0 A - 3RV_{\text{air}}^2)\cos 2\omega_0 t \right. \\ \left. + 2A^2 \cos^2 2\omega_0 t\right). \tag{13}$$

As can be seen from (13), the vibratory component consists of the second-order and fourth order vibrations related with the fundamental rotational speed ω_0. If the amplitude A is not zero, the fourth-order component cannot be zero. On the

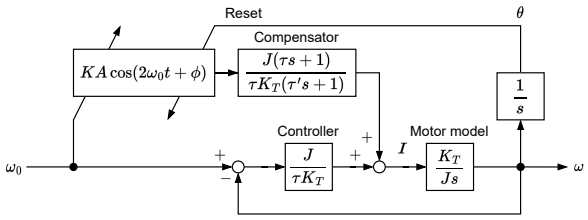

Fig. 2. Block diagram of proposed vibration reduction by higher harmonic rotational speed control method.

other hand,the second-order component can be zero when the following equation is satisfied:

$$A = \frac{3V_{\text{air}}^2}{4R^2\omega_0} \tag{14}$$

and the vibratory component is

$$F_{z\theta} = \frac{1}{6}\rho C_L C\left(2A^2\cos^2 2\omega_0 t\right) \tag{15}$$

$$= \frac{1}{6}\rho C_L C A^2(1-\cos 4\omega_0 t) \tag{16}$$

Now, since the rotational speed is sufficiently high and the tip speed $R\omega$ is much faster than the crosswind speed V_{air}, it can be observed that the amplitude of the fourth harmonic component after the harmonic input is much smaller compared to the second harmonic component before the harmonic input. In this case, the input waveform approximately $\cos 2\theta$, causing vibrations to decrease due to a waveform that moves quickly along the flow direction and slowly in the vertical direction.

In the actual rotors, the rotational speed harmonic input (7) is input as a command value considering the delay in the rotational speed control system. The block diagram of the controller design, where the rotational speed harmonic input is provided as a feedforward command value to the motor, is shown in Fig. 2, where J is inertia of the rotor, τ is the time constant of the rotational speed control, and τ' is the time constant for compensator. The rotational speed control is designed assuming a nominal model without viscous friction. The harmonic input is input as a command value through a compensator for the delay in the rotational speed control loop. This allows exploiting the high responsiveness of motor torque via current command values.

While in the model the phase is defined as the rotational angle with the wind direction as 0 and the amplitude is determined by the model as (14), in real application, the value of the harmonic rotational speed input that minimizes the amplitude is affected by model errors. Hence, correction parameters to the amplitude K and phase ϕ are added. Here, the command value of the rotational speed is implemented as

$$\omega = \omega_0 + KA\cos(2\omega_0 t+\phi) \tag{17}$$

and the coefficients K, ϕ for the correction use the values that are measured in advance and kept as maps.

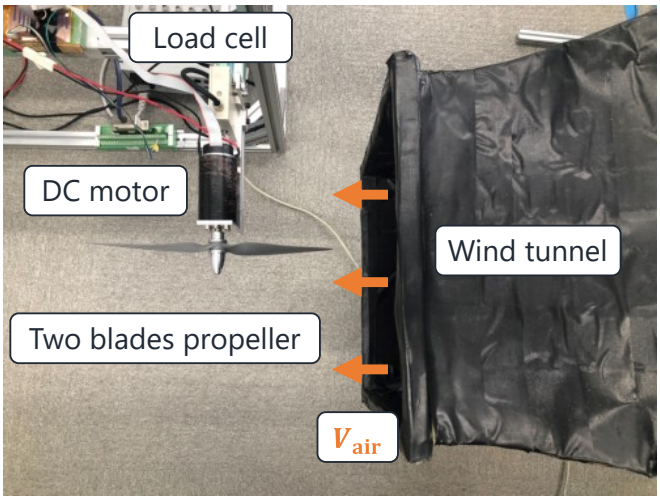

Fig. 3. Experimental setup of single small rotor and wind tunnel.

TABLE I
SCALE ROTOR PARAMETERS.

Parameter	Value
Propeller radius R	12.5 cm
Average chord length C	1.5 cm
Number of the blade b	2
Lift coefficient C_L	0.53
Drag coefficient C_D	0.7
Inertia of the rotor J	1.3×10^{-4} kgm^2

C. Experimental setup

The effectiveness of the proposed method is validated by the experiment using a rotor bench which assumes the small sized multirotors. Experimental setup is shown in Fig. 3. The experimental setup is consists of the propeller, the motor, the load cell, and the simple wind tunnel. The load cell is capable of measuring a uniaxial force in the direction of thrust, either tension or compression. The parameters of the experimental setup are shown in Table I.

D. Conditions of validation

The verification process began by confirming the vibration generated by the rotor under both calm and crosswind conditions. Subsequently, the proposed method was experimentally validated by measuring vibrations under various parameter conditions to determine the optimal parameters. The effectiveness of the proposed method was then evaluated using the optimal conditions obtained.

The conditions for measuring rotor thrust under calm and crosswind conditions are presented in Table II.

The measuring conditions for the experimental validation

TABLE II
SCALE ROTOR VIBRATION MEASUREMENT CONDITION.

Parameter	Value
Wind velocity V_{air}	5 m s^{-1}
Measuring time	1 s
Number of measurements	100

TABLE III

SCALE ROTOR PARAMETERS.

Parameter	Value
Rotational speed n	10 rps to 50 rps by 5 rps
Current limit I	5 A
Phase offset ϕ	$-90°$ to $90°$ by $10°$
Amplitude gain K	0.1 to 1 by 0.1
Measurement length of each case	1 s
Number of measurement of each case	10
Time constant of rotational speed control τ	0.1 s
Time constant of compensator τ'	0.003 s

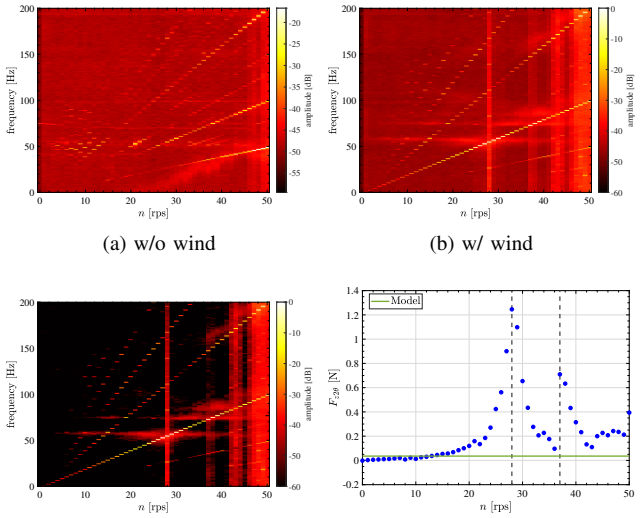

(a) w/o wind

(b) w/ wind

(c) Difference between w/ and w/o wind condition.

(d) Difference between w/ and w/o wind condition at second-order vibration. The supposed resonance points are shown in gray lines.

Fig. 4. Tracking map of experimental results of forces.

of the proposed method are shown in Table III. Here, n stands for rotational speed in rps, thus $\omega = 2\pi n$. The amplitude gain was selected to ensure that the amplitude of the current does not saturate.

III. RESULTS OF EXPERIMENTAL VALIDATION

A. Measurement results of crossewind-induced vibrations

The measured vibrations of the thrust F_z were analyzed using tracking analysis, which is commonly employed in vibration analysis of rotating body. The results are shown in Fig. 4 The FFT results of the measured data at constant rotational speeds are arranged horizontally with the vibration frequency on the vertical axis.

The vibration without wind is shown in Fig. 4a, The vibration with crosswind is shown in Fig. 4b, and the difference between the two conditions is shown in Fig. 4c. Additionally, the variation of the second-order vibration corresponding to the blade number times the rotational speed expected from the model is shown in Fig. 4d.

From Fig. 4, it is evident that there is strong vibration at the second harmonic of the rotational speed. Mainly, at 25 rps and 37 rps, the second-order harmonic is near resonance, significant vibration occurs, and modulation of vibration is observed at frequencies other than 50 Hz. The vibration depicted in Fig. 4c corresponds to the component of increased vibration due to crosswind inflow. In practical drones, this vibration occurs when the drone encounters crosswinds or when it has a relative velocity to the airflow. The model predicts that the second-order vibration remains constant regardless of rotational speed. However, as seen in Fig. 4d, the measured data exhibit peaks in vibration intensity. The cause of this discrepancy can be attributed to the mechanical resonance inherent in the the measurement system.

TABLE IV

CONDITIONS OF MINIMUM VIBRATION IN EACH ROTATIONAL SPEED.

n [rps]	10	15	20	25	30	35	40	45	50
ϕ [deg]	-50	-70	-70	-30	10	-40	-10	80	30
K [-]	0.1	0.1	0.1	0.1	0.6	0.1	0.6	0.4	0.8

B. Results of effectiveness validation of the proposed method

The verification results of the proposed method to reduce the second-order thrust vibration corresponding to the rotational speed are shown and described here. The average thrust remained almost unchanged regardless of the presence of the proposed method. Therefore, only the results of the vibration are going to be considered.

Firstly, the optimal phase ϕ and amplitude K are examined among all conditions. The measured values at each rotational speed were FFT analyzed, and the amplitudes of the vibrations corresponding to the second order of rotational speed were mapped for each ϕ, K combination, as shown in Fig. 5. The conditions where the second order vibration is minimized at each rotational speed based on the map in Fig. 5 are presented in Table IV. The vibration levels when applying the proposed method of higher harmonic rotational speed input under the conditions of minimum amplitude are compared with both crosswind and no-wind conditions. This comparison is shown in Fig. 6.

Fig. 7 illustrates the vibration levels and the frequency-domain values obtained by FFT under crosswind conditions when applying the harmonic rotational speed input at the conditions of minimum amplitude. From Fig. 5, Fig. 6, and Fig. 7, it is evident that the proposed method effectively reduces the second-order vibrations other than 10 rps. Particularly, the effect of the proposed method is significant for the vibrations at 25 rps and 50 rps under the crosswind conditions, as observed in the measurement results of vibration shown in Fig. 4d, where the vibrations are amplified due to the mechanical resonance, especially when the rotational speed corresponds to the second or fundamental harmonic at 50 Hz. However, the amount of change in vibration varies with rotational speed, and it differs from the increase predicted by the model. This discrepancy suggests the presence of mechanical resonance in the measurement system, as discussed in the modeling and experimental measurements section, highlighting the need to further investigate the combined effect of mechanical resonance and vibration suppression.

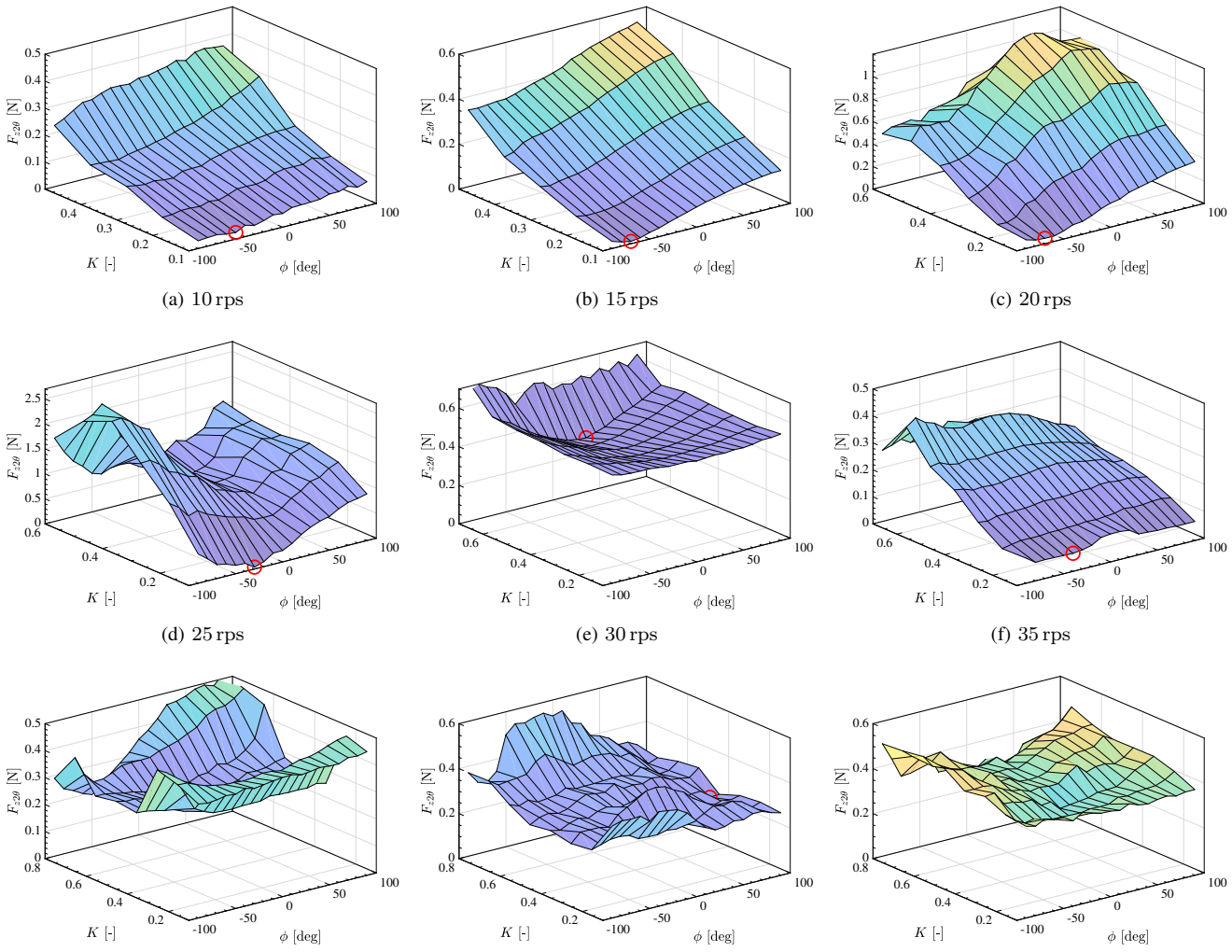

(a) 10 rps (b) 15 rps (c) 20 rps

(d) 25 rps (e) 30 rps (f) 35 rps

(g) 40 rps (h) 45 rps (i) 50 rps

Fig. 5. 2nd order vibration amplitude in various gains and phases of higher harmonic rotational speed control. The red circles are the minimum point.

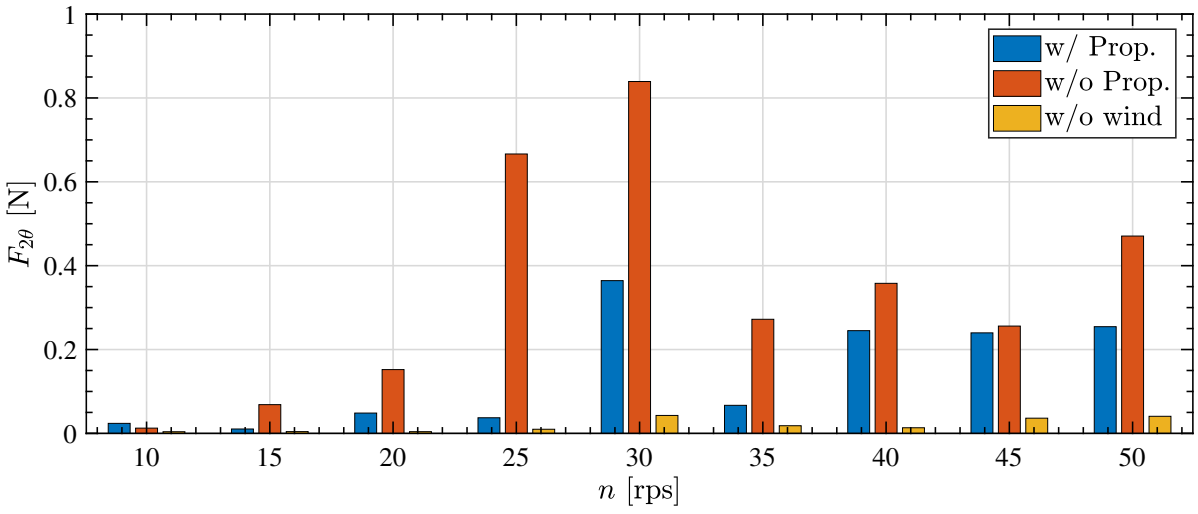

Fig. 6. Comparison of 2nd order vibration amplitude of proposal at best condition, without proposal, and without wind cases.

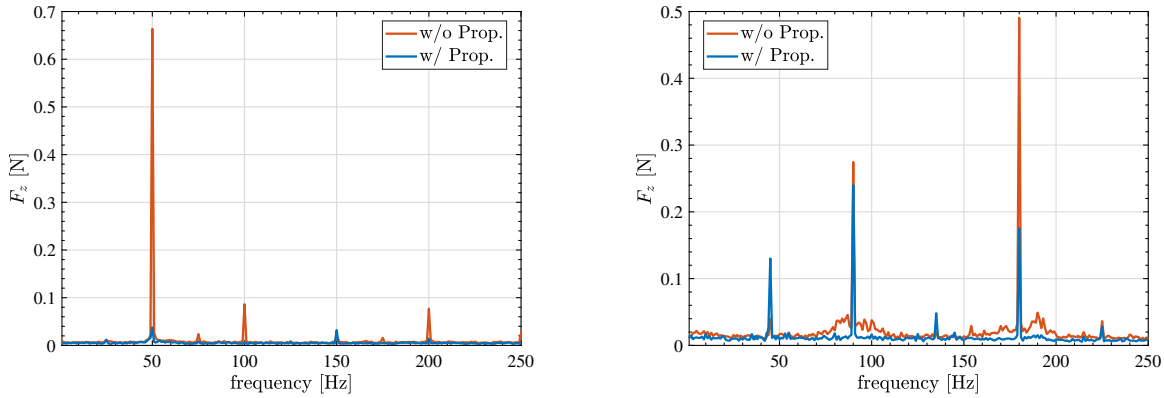

(a) 25 rps: the most effective case.

(b) 45 rps: the least effective case except for 10 rps.

Fig. 7. The frequency spectrum results with the proposal in the best parameters and without the proposal.

Regarding the issue of increased vibration at 10 rps, it is apparent from Fig. 6 that the vibration itself is very small, and the effect of the proposed method is not evident. Moreover, while the model predicted an increase in the fourth-order vibration for vibrations other than the second-order, it is observed from Fig. 7 that it actually decreases. It is expected that at 25 rps, the resonance at 50 Hz is reduced, and at 45 rps, the resonance near 170 Hz is mitigated, suggesting the need for further verification.

IV. Conclusion

This paper proposes thrust vibration suppression method using harmonic rotational speed input. There is a problem of mechanical vibration occurring in situations where the relative wind vector varies depending on the rotational position. Therefore, in this study, we aimed to reduce the aerodynamic vibration of thrust during crosswind conditions by applying higher harmonic rotational speed inputs.

The forces acting on propellers in crosswind conditions were modelled. Experiments were conducted in a wind tunnel under constant wind speed conditions. The observed vibration amplitude was larger than predicted by the model, indicating the presence of other mechanical factors.

The proposed method is based on the model. The correction terms were introduced to compensate for model errors. The effectiveness of the proposed method was experimentally validated. The correction terms were swept to determine the optimal harmonic input. It was confirmed that it is possible to select appropriate input parameters and observed that the optimal conditions vary for each rotational speed. The proposed method was confirmed to be effectively generate inputs for vibration reduction by pre-mapping or creating a database of vibration reducing inputs.

The proposed method is expected to suppress vibration sources independently of vibration control in the aircraft level by applying it to multirotors such as UAVs. Future work include considering vibrations and torque fluctuations in other axes, as well as addressing mechanical resonance. Furthermore, verification of the proposed method under different scales and wind speeds remains to be explored.

References

[1] K. Nonami, "Drone technology, cutting-edge drone business, and future prospects." *Journal of Robotics and Mechatronics*, vol. 28, no. 3, pp. 262–272, 2016.

[2] T. Zimbelman, L. Dailey, D. Oriach, N. Flom, and M. Metcalfe, "Advanced air mobility missions for public good," National Aeronautics and Space Administration, Tech. Rep., 2023.

[3] K. Yokota and H. Fujimoto, "Aerodynamic force control for tilt-wing evtol using airflow vector estimation," *IEEE Transactions on Transportation Electrification*, vol. 8, no. 4, pp. 4163–4172, 2022.

[4] F. Tauro, C. Pagano, P. Phamduy, S. Grimaldi, and M. Porfiri, "Large-scale particle image velocimetry from an unmanned aerial vehicle," *IEEE/ASME Trans. Mechatronics*, vol. 20, no. 6, pp. 3269–3275, 2015.

[5] F. Beltran-Carbajal, H. Yañez-Badillo, R. Tapia-Olvera, A. Favela-Contreras, A. Valderrabano-Gonzalez, and I. Lopez-Garcia, "On active vibration absorption in motion control of a quadrotor uav," *Mathematics*, vol. 10, no. 2, 2022.

[6] S. Bennaceur and N. Azouz, "Modelling and control of a quadrotor with flexible arms," *Alexandria Engineering Journal*, vol. 65, pp. 209–231, 2023.

[7] T. Maki, M. Zhao, K. Okada, and M. Inaba, "Elastic vibration suppression control for multilinked aerial robot using redundant degrees-of-freedom of thrust force," *IEEE Robotics and Automation Letters*, vol. 7, no. 2, pp. 2859–2866, 2022.

[8] K. Yokota and H. Fujimoto, "Pitch angle control by regenerative air brake for electric aircraft," *IEEJ Journal of Industry Applications*, vol. 11, no. 2, pp. 308–316, 2022.

[9] P. P. Friedmann and T. A. Millott, "Vibration reduction in rotorcraft using active control - a comparison of various approaches," *Journal of Guidance, Control, and Dynamics*, vol. 18, no. 4, pp. 664–673, 1995. [Online]. Available: https://doi.org/10.2514/3.21445

[10] D. Patt, L. Liu, J. Chandrasekar, D. S. Bernstein, and P. P. Friedmann, "Higher-harmonic-control algorithm for helicopter vibration reduction revisited," *Journal of guidance, control, and dynamics*, vol. 28, no. 5, pp. 918–930, 2005.

[11] T. R. Norman, C. Theodore, P. Shinoda, D. Fuerst, U. T. Arnold, S. Makinen, P. Lorber, and J. O'Neill, "Full-scale wind tunnel test of a uh-60 individual blade control system for performance improvement and vibration, loads, and noise control," in *American Helicopter Society 65th Annual Forum, Grapevine, TX*, 2009.

[12] S. F. Toloue, S. H. Kamali, and M. Moallem, "Torque ripple minimization and control of a permanent magnet synchronous motor using multiobjective extremum seeking," *IEEE/ASME Trans. Mechatronics*, vol. 24, no. 5, pp. 2151–2160, 2019.

[13] S.-H. Park, J.-C. Park, S.-W. Hwang, J.-H. Kim, H.-J. Park, and M.-S. Lim, "Suppression of torque ripple caused by misalignment of the gearbox by using harmonic current injection method," *IEEE/ASME Trans. Mechatronics*, vol. 25, no. 4, pp. 1990–1999, 2020.

[14] Y. Tsuji, D. Yashiro, Y. Kato, S. Bando, K. Yubai, and S. Komada, "Design of a thrust controller for propeller driven systems operating at multiple wind velocities and propeller angular velocities," *IEEJ Journal of Industry Applications*, vol. 12, no. 6, pp. 1060–1067, 2023.